Bimodal palm biometric feature extraction using a single RGB image

Teodors Eglitis, Mihails Pudzs, Modris Greitans
Institute of Electronics and Computer Science
14 Dzerbenes Street, Riga, LV1006, Latvia
Teodors.Eglitis@edi.lv; Mihails.Pudzs@edi.lv; Modris.Greitans@edi.lv

Abstract: This paper proposes a method for palm bimodal biometric feature (vein and crease pattern) acquisition from a single RGB image. Typical bimodal biometric systems require combining infrared and visible images for this task. We use a single CMOS color sensor and a specific illumination comprising of two wavelengths to acquire the image. As a result each biometric modality is more pronounced in its own color channel. The image is processed by applying adapted matched filters with nonlinear modifications. Performance of the proposed method is evaluated against feature separation with optical band-pass and band-stop approach on a database of 64 people. The results show the average true positive rate is $70.6\ \%$ for vein detection and $64.7\ \%$ for crease detection, whereas in $14.8\ \%$ and $9.29\ \%$ of the cases feature of wrong modality is detected.

1 Introduction

It is difficult to spoof human palm blood vessel structure as biometric feature because one can't leave his or her "blood vessel print" on a surface, unlike fingerprints. This has motivated studies and manufacturing of vascular biometric systems [WESS05]. More than one biometric feature (multimodal biometry) is used to increase biometric system's level of security. There are such multimodal biometric systems that use palm blood vessel structure and palm prints by analyzing two images in visible and infrared light. The disadvantage of these systems is that two images must be acquired: either sequentially, using mechanically-switched optical filters [PFR+13], or simultaneously, using two image sensors [MCJ10]. This is because each biometric parameter requires different light spectrum — palm crease images are obtainable at $390 \cdots 700\ nm$ while blood vessel images require near-infrared light spectrum — wavelengths longer than $750\ nm$ [SB99].
In this paper we propose a method for palm biometric features of two modalities (vein pattern and crease structure) extraction of a single image. We use spectral properties of the chosen biometric features and acquire images where the features of each modality appear more pronounced in separate color channels. This is described in section 2. The acquired images are then digitally processed. The state of the art methods for palm feature extraction employ contrast enhancement and binarization [AEHS13]. However, these methods are not suitable for the proposed task. Therefore, we use filters developed by Pudzs et al. [PGF11], and adapt them to extract biometric features of each modality separately, as de-

scribed in section 4. In sections 5 and 6 the proposed approach is validated experimentally — we measure how often can crease and vein features be distinguished.

2 Palm feature spectral separation

Each color channel of a typical CMOS sensor with RGB color filter array (Bayer filter) is sensitive to near-infrared light in addition to its sensitivity in the corresponding light spectrum [Tru12]. In this section we show how to exploit this property to pronounce

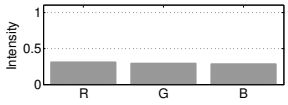

(a) only near-infrared illumination

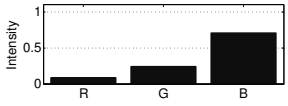

(b) only blue illumination

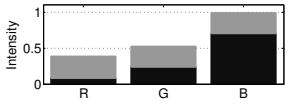

(c) dichromatic illumination

Figure 1: Pixel intensity distribution in color channels (example)

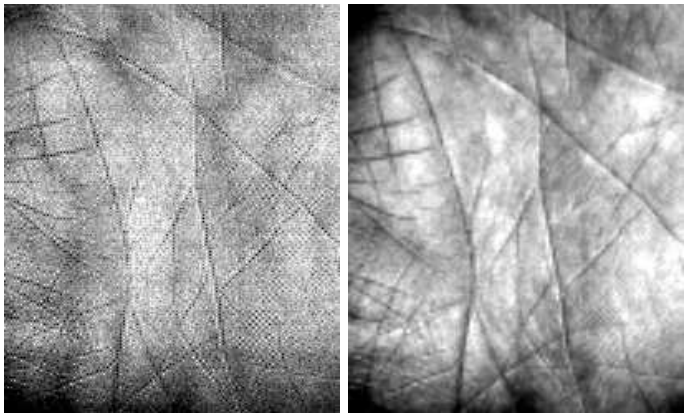

(a) red channel (b) blue channel

Figure 2: Palm image fragment in proposed lighting conditions (example; contrast was enhanced for visualization purposes)

features of each modality in different color channel. The choice of RGB channels depends on the spectrum sensitivity of the used image sensor. In our model we use *Aptina MT9V032C12STC ES* RGB image sensor because it complies with our demanded quantum efficiency [Apt11] in relevant spectrum bands and it is widely available, and we use R and B color channels for vein and crease features respectively. For any other image acquisition system there might be different considerations over which color channels to use, depending on the sensor and illumination device, but the general technique remains the same. Since all color channels of the image sensor have similar sensitivity to near-infrared spectrum, when palm is illuminated with near-infrared light, information from this wavelength (vein pattern) is recorded in all 3 color channels. An example of pixel intensity distribution in the RGB color channels can be observed in figure 1a. When palm is illuminated with monochromatic visible light (in our case — blue), information from this wavelength (crease pattern) is recorded mostly in the corresponding RGB channel — an example of pixel intensity distribution can be observed in figure 1b. Therefore, when both of the mentioned light sources are simultaneously applied with different intensities, different color channels (in our example — R and B) will contain information mostly observed

in each light separately. An example of pixel intensity distribution for dichromatic light can be observed in figure 1c. Thus, palm veins will be mostly visible in red channel, while palm crease structure — mostly in blue channel. The red channel was selected for palm vein information recording because it has the highest sensitivity in near-infrared spectrum between all color channels. Blue channel was chosen for crease information recording because of its smallest overlap with the red channel in visible light spectrum band [Apt11]. Our experiments with images verified that it is possible to find a pair of simultaneous illumination intensities to achieve the desired effect. Such illumination used for captured image, fragment of which is shown in figure 2. Fig. 2a shows the red channel pixels, while 2b shows the blue channel pixels. Notice that the former appears to contain visually more expressed veins and the latter — more expressed crease, however, this is not sufficient for bi-modal feature extraction.

3 Palm crease and blood vessel model

This section discusses the methods for distinguishing between creases and veins in palm images. The apparent differences of these features are their visual appearance which will

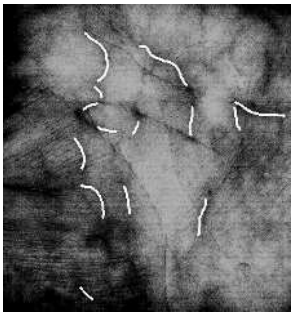

(a) Palm image fragment with manually labeled veins

(b) Palm image fragment with manually labeled creases

(c) Vein CF, taken from 3a

(d) Crease CF, taken from 3b

Figure 3: An example of vein/crease CF acquisition (contrast was enhanced in all images for visualization purposes)

be analyzed in this section. Therefore we have created a database of palm images that are acquired in the mentioned lighting conditions, and manually labeled distinct fragments of palm features (fig. 3a, 3b). Selected feature fragments are straightened and concatenated together to form a continuous feature (CF) — fig. 3c, 3d. From these statistics crease and blood vessel average CF models (ACFM) were obtained for each RGB color channel, fig. 4a and 4b respectively. To display each feature RGB ACFM in one picture, it is assumed that each feature's color channel's ambient pixels have value 1. As intended, palm blood vessels appear more strongly (darker) in red channel, but palm crease — in blue channel, but both are also seen in other color channels with lower magnitude. Also the claim that these biometric features have different width was confirmed — typical marked palm blood

vessel width in red channel is greater than 10 pixels, but palm ridge width is approximately $3 \cdots 6$ pixels (in captured images with system that is being developed, placing palm at about the same distance). When placing palm in a different distance from the camera feature width might be different, but their ratio shall remain the same. These appear to be sufficient differences for palm blood vessels and crease separation using matched filters.

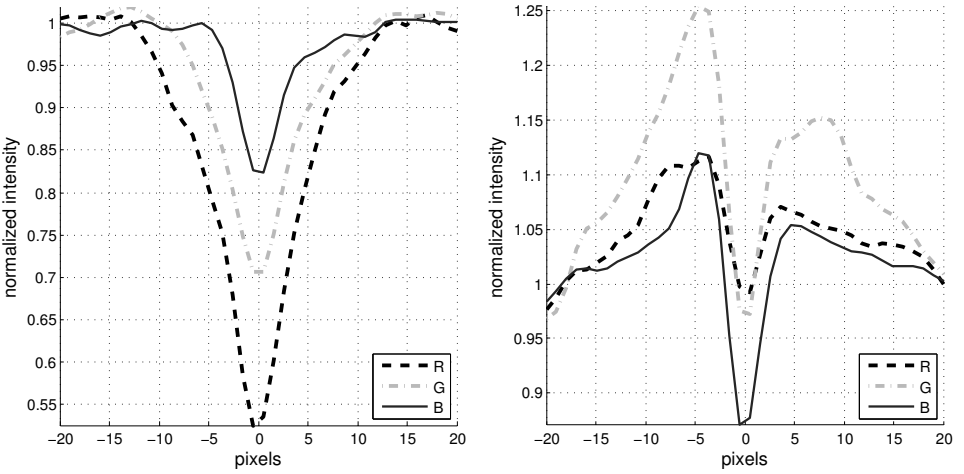

(a) veins (b) creases

Figure 4: Average palm vein and crease ACFM for each color channel of RGB image

4 Filter development

Both feature detection filters must extract lines with certain thickness, therefore in sec. 4.1 and 4.2 we are focusing on development of a universal filter for this purpose. Development of such matched filter (MF) is discussed using a benchmark test image — fig. 6a. The goal is to extract lines with certain width as defined by the outlined region in the image. As every real palm image would, this image contains narrower and wider lines as well as gradients and patterns that are considered as noise.
Subsequently in sections 4.3 and 4.4 we will discuss filter parameters and modifications that are distinct for vein and crease detection.

4.1 Filter structure and its response

The filter structure and its response is based on the NH-CMF (Non-Halo Complex Matched Filter) introduced in [PGF11]. The idea behind the NH-CMF is that the filter kernel (fig. 5a) is matched with a line-like object (LLO) one wants to extract. The kernel is rotated

in angular interval $\varphi_n \in [0,\ \pi)$, using uniformly distributed N rotations (e.g. $N = 4$). Filter response R_{NH} at particular point $(x_0,\ y_0)$ with kernel rotation angle φ_n is defined as:

$$R_{\mathrm{NH}_{(x_0,\ y_0,\ \varphi_n)}} = \mathrm{ramp}\left[\iint_D f(x,y)\cdot M(x-x_0, y-y_0; \varphi_n)\cdot dxdy\right] \tag{1}$$

where $f(x,y)$ is the image being filtered and D is the overlay area of the kernel M, and $\mathrm{ramp}\,(x) = \frac{x+|x|}{2}$. The kernel is constructed so that it has no mean value, meaning zero response for mean component of $f\,(x,y)$, within D. Negative responses for each φ_n are converted to 0 because such responses indicate that the particular image region at the given angle φ_n does not represent requested LLO. Each point's $(x_0,\ y_0)$ N responses are combined using complex numbers (c.f. [PGF11], section V.). Without dwelling deeper in NH-CMF we describe the approach to adapt the filter for the required task (selective line detection). Filter kernel can be divided into segments without altering its size or principle of operation — fig. 5b. It is divided into 10 segments placed in 2 columns ($N_B = 2$), to perform line continuity test, and 5 rows ($N_A = 5$), to determine line width (the reason for such segmentation is discussed in corresponding sub-sections 4.2.1 and 4.2.2). Segments are labeled as $A_a\ B_b$ for convenience (refer to fig. 5b). Each mask segment's $A_a\ B_b$ correlation $S_{(a\ b)}$ with an underlying image fragment is calculated as:

$$S_{(a\ b)\ (x_0,\ y_0,\ \varphi_n)} = \iint_{A_a\ B_b} f(x,y)\cdot M(x-x_0, y-y_0; \varphi_n)\cdot dxdy\ . \tag{2}$$

Hereafter in most equations variables $x_0,\ y_0,\ \varphi_n$ are left out. Filter response remains the same, but now equation (1) can be rewritten using segment responses $S_{(a\ b)}$:

$$R_{\mathrm{NH}} = \mathrm{ramp}\left[\sum_{b=1}^{2}\left(3\cdot\left(S_{(1\ b)} + S_{(5\ b)}\right) - 2\cdot\sum_{a=2}^{4} S_{(a\ b)}\right)\right]\ . \tag{3}$$

Such NH-CMF response R_{NH} on an artificial test image (fig. 6a) can be seen in fig. 6b. In the next subsections we iteratively improve the quality of NH-CMF result (fig. 6b) for the specified task by removing unwanted responses (denoted as *artifacts*). Therefore, our proposed filter consists of a non-linear NH-CMF with a modified kernel and an additional calculation module for artifact removal.

4.2 Artifact removal

Various objects, other than necessary features, processed with NH-CMF will give non-zero filter output responses because their shape is remotely similar to object with which filter is matched — artifacts. Artifact removal is performed at each kernel's rotation angle φ_n, before responses are combined for each individual image point — $(x_0,\ y_0)$. Non-Artifact check variable C is defined as:

$$C = C_{\mathrm{C}}\cdot C_{\mathrm{W}}\cdot C_{\mathrm{G1}}\cdot C_{\mathrm{G2}}\ , \tag{4}$$

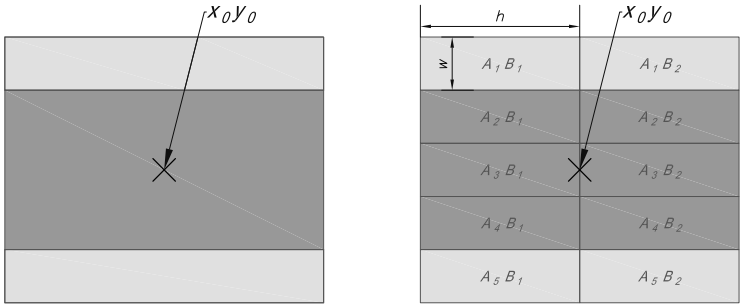

(a) NH-CMF filter kernel ([PGF11])

(b) The proposed division of NH-CMF filter kernel into 10 segments

Figure 5: NH-CMF filter kernel and its proposed division into 10 segments

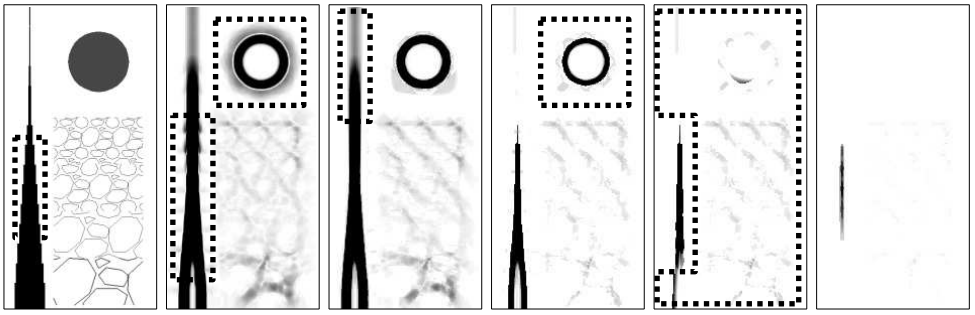

(a) Original image

(b) R_{NH}

(c) $R_{\mathrm{NH}} \cdot C_{\mathrm{C}}$

(d) $R_{\mathrm{NH}} \cdot C_{\mathrm{C}} \cdot C_{\mathrm{W}}$

(e) $R_{\mathrm{NH}} \cdot C_{\mathrm{C}} \cdot C_{\mathrm{W}} \cdot C_{\mathrm{G1}}$

(f) $R_{\mathrm{NH}} \cdot C$

Figure 6: Test image and filtration results, the processed images (6b-6f) are inverted (darker region represents a higher correlation with the filter kernel), black picture borders are not part of the data, but added for convenience

and it can take values 0 and 1: 0 when given filter output value can be recognized as artifact and 1 — otherwise. Its constituent variables $C_{\mathrm{C}}, C_{\mathrm{W}}, C_{\mathrm{G1}}$ and C_{G2} can also take values 0 and 1, and are discussed in the following chapters. Proposed filter response for one kernel's rotation angle is:

$$R_{\mathrm{final}(x_0,\, y_0,\, \varphi_n)} = R_{\mathrm{NH}(x_0,\, y_0,\, \varphi_n)} \cdot C_{\,(x_0,\, y_0,\, \varphi_n)} \,. \tag{5}$$

4.2.1 Line continuity

As it can be seen in marked regions in fig. 6b, the filter has a non-zero correlation around lines and gradients. Such response emerges when kernel's rotation angle φ_n forms a certain oblique angle Δ with LLO's direction so that kernel only partly overlays LLO. Such filter responses can be detected by dividing the filter kernel in two columns (two is the minimum number of columns, using larger number will also examine whether the line is continuous in its intermediate sections) — in fig. 5b these 2 columns are formed by segments $A_a\boldsymbol{B_1}$ and $A_a\boldsymbol{B_2}$, perceiving each column B_b as a separate matched filter.

$$(\forall b \in \{1,2\}) \quad R_{\mathrm{C}_b} = \mathrm{ramp}\left[3 \cdot \left(S_{(1\ b)} + S_{(5\ b)}\right) - \sum_{a=2}^{4} S_{(a\ b)}\right] \tag{6}$$

We are interested only in binary operator C_{C}, therefore line continuity test can be performed:

$$C_{\mathrm{C}} = \mathrm{H}\left[\min\left(R_{\mathrm{C}_b}\right)\right] \,, \tag{7}$$

where H function is defined as follows:

$$\mathrm{H} = \begin{cases} 0, & \text{if } x \leqslant 0 \\ 1, & \text{if } x > 0 \,. \end{cases} \tag{8}$$

The performance of NH-CMF with added line continuity check (with a response restricted by $R = R_{\mathrm{NH}} \cdot C_{\mathrm{C}}$) on a test image fig. 6a can be seen in 6c. Notice that mentioned artifacts have been partially removed.

4.2.2 Line width

Specified line width is one of the key features for crease / vein separation as discussed in section 3. Although filter is matched with *thick* lines, it can be noticed that filter output response depends also on kernel's geometry, not only the input signal, as marked in fig. 6c. If line is several times thinner than the kernel's dark region, there are going to be multiple x coordinates $(x_n \cdots x_m,\ y_0)$ (in case of a vertical line) where the filter kernel's center can be placed in order to obtain positive output response. Such thin line in NH-CMF output will result in a positive response region whose width is approximately equivalent to kernel's negative region width.
To allow detect only lines with a specific width (greater than few pixels) the line compatibility with filter kernel can be verified in multiple line's cross section points. This can be

achieved by dividing kernel's dark region into rows. Lets look at column B_1. It consists of 2 positive segments (A_1B_1 and A_5B_1) and kernel's dark (negative) part is divided into 3 segments — A_2B_1 to A_4B_1 (2 is the minimum number of segments but 3 segments are chosen experimentally. The maximum number of such segments depends on line's width in pixels.). Whether line has allowed thickness value, can be determined by checking if under each negative filter kernel's segment is a "part of line" carrying out a "partial matching". It can be done as follows:

$$(\forall a \in \{2,3,4\})\,(\forall b \in \{1,2\}) \quad R_{\mathrm{W}_{a,\,b}} = \mathrm{ramp}\left[S_{(1\;b)} + S_{(5\;b)} - 2 \cdot S_{(a\;b)}\right] \tag{9}$$

As before, we need to obtain binary C_{W} merging all 6 individual segment results: $R_{\mathrm{W}_{a,\,b}}$:

$$C_{\mathrm{W}} = \mathrm{H}\left[\min\left(R_{\mathrm{W}_{a,\,b}}\right)\right] \ . \tag{10}$$

Response obtained using line continuity and width checks ($R = R_{\mathrm{NH}} \cdot C_{\mathrm{C}} \cdot C_{\mathrm{W}}$) can be seen in fig. 6d.

4.2.3 Gradient checks

So far, all viewed filters detect gradients along with lines (hence the term LLO was used). When performing line continuity check, each kernel column's negative segment $S_{(2\;b)} \cdots S_{(4\;b)}$ is viewed in conjunction with both positive side segments — $S_{(1\;b)}$ and $S_{(5\;b)}$ to determine if there is an LLO. When filter kernel is located on top of a gradient, alongside it, filter result (at the given angle) will be non-zero because partially matched filter requirements will be met. However, following operation results for $\forall b$, $a = 1$ and $a = 5$ simultaneously won't be non-zero:

$$(\forall a \in \{1,5\})\,(\forall b \in \{1,2\}) \quad R_{\mathrm{G1}_{a,\,b}} = \mathrm{ramp}\left[3 \cdot S_{(a\;b)} - \sum_{i=2}^{4} S_{(i\;b)}\right] \tag{11}$$

because, in case of a gradient, under one of these segment combinations a reverse gradient or a constant image pixel values will be located. The gradient test — G1 can be performed to both filter columns by calculating:

$$C_{\mathrm{G1}} = \mathrm{H}\left[\min\left(R_{\mathrm{G1}_{a,\,b}}\right)\right] \ . \tag{12}$$

NH-CMF output result with added C_{G1} check can be seen in fig. 6e — gradient formed artifacts (marked regions in fig. 6d) have been removed. However, part of the *random* artifacts from the marked region in fig. 6e can be classified into groups that have already been observed in the previous chapters. In order to enhance ability to distinguish valid signal from them, gradient check G2 is introduced. This test is performed by requesting each kernel's negative segments ($(\forall a \in \{2,3,4\})\,,\ (\forall b \in \{1,2\})$) to form a positive result with its corresponding positive side segments as follows:

$$\begin{aligned}(\forall a \in \{2,3,4\})\,(\forall b \in \{1,2\})\; R_{\mathrm{G2}_{1_{a,\,b}}} &= \mathrm{ramp}\left(S_{(1\;b)} - S_{(a\;b)}\right) \\ R_{\mathrm{G2}_{2_{a,\,b}}} &= \mathrm{ramp}\left(S_{(5\;b)} - S_{(a\;b)}\right) \ ,\end{aligned} \tag{13}$$

from which it is understandable that gradient check 2 variable C_{G2} can be defined:

$$C_{\mathrm{G2}} = \mathrm{H}\left[\min\left(R_{\mathrm{G2}1_{a,\ b}}\ ,\ R_{\mathrm{G2}2_{a,\ b}}\right)\right]\ . \tag{14}$$

Analyzing equations (13) and (14), it can be seen that condition C_{G2} includes (or *is stronger than*) previously viewed checks — C_{C}, C_{W} and C_{G1}, which means that eq. (4) can be rewritten as $C = C_{\mathrm{G2}}$. This claim can be verified by observing filter responses in fig. 6f.

4.3 Blood vessel filter

So far we examined filter structure for executing the set of tests for artifact removal — a general case. To describe specific filters that are matched with previously defined palm vein and crease width, we introduce variables that describe kernel's segment dimensions — fig. 5b — h - segment length and w - segment width.
Since veins comply with previously predefined characteristics as "thick lines", it is only necessary to scale the developed filter kernel from fig. 5b — experimentally determined that optimal results are achieved if $h = 11$ and $w = 5$ for the particular system. Such filter output response (detected palm veins) for input RGB image from fig. 2 is shown in fig. 7, marked as ■.

Figure 7: Input RGB image from figure 2 processed by the proposed filters (responses (vein - ■, crease - ■) are drawn over grayscale image)

4.4 Crease filter

In section 3 it was shown that marked ridges (only widest and more clearly visible were marked) are approximately $3 \cdots 6$ pixels wide. It means that smaller palm prints are $1 \cdots 2$ pixels wide — not only palm print width difference can be approx. $6\times$, but also crease filter kernel's dark region can't be divided into multiple rows (for example, one pixel wide crease can't be detected in this way). Therefore, it is proposed to use opposite approach to line width test — instead of checking if line is under kernel's multiple negative segments (in line width direction), allowing the line to be only under the central negative segment in each column — now segment results $A_2\ B_b$ and $A_4\ B_b$ (fig. 5b) are ignored — both calculating R_{NH} and performing artifact checks. This also provides resembling output magnitude to different width lines. Experiments determined that using such filter for crease detection, optimal filter parameters are $h = 2$ and $w = 2$. Filter output response (detected palm ridges) for input image 2b is shown in fig. 7, marked as ■.

5 Experiments

In our experiments it is assumed that the optical method (using bandpass/bandstop light filters), which is used in other biometric systems, provides maximum separation of palm biometric modalities. Therefore, it is used as a benchmark for evaluation of our proposed method, which is aimed to accomplish the same task — feature separation. We evaluate method's ability to: 1) detect each feature, and 2) distinguish features of different modalities. This is done by calculating the True Positive (TP) and False Positive (FP) detection rates of proposed filters.

Data

We have acquired a database of 64 people (age 22 — 79) palm images. For each person 30 images were taken in our proposed lighting conditions. In addition, two ground truth images for each person were acquired using optical filters — one in near-infrared light to represent pure vein structure, and the other — in blue light representing pure crease structure.

Evaluation Method

The magnitude of filter response is proportional to the detail's correlation with the filter kernel — higher magnitude denotes more expressed palm feature, which is essential for the feature comparison algorithm. Due to the nature of our feature comparison algorithm, which takes magnitude of detected features into account, we preserve this information and use *Magnitude-Weighted Histogram* (MWH) [PFG13] method for evaluation. The most convenient way to calculate MWH is to sum filtered images that are properly aligned. Each MWH pixel contains information of how often and how significantly filter responds in it.

Experimental Procedure

MWHs were calculated for each modality and every person — a total of 2×64 MWH images. For convenience, let us denote MWH images for analyzed person as $\mathrm{MWH}_{\mathrm{vein}}(x,\ y)$ and $\mathrm{MWH}_{\mathrm{crease}}(x,\ y)$. Ground truth images were processed and binarized to acquire ground truth masks — $\mathrm{GT}_{\mathrm{vein}}(x,\ y)$ and $\mathrm{GT}_{\mathrm{crease}}(x,\ y)$. Using these masks we are able to calculate TP rates of our proposed filters in the following manner:

$$\mathrm{TP}_{\mathrm{vein}} = \frac{\sum_x \sum_y \mathrm{MWH}_{\mathrm{vein}}(x,\ y) \cdot \mathrm{GT}_{\mathrm{vein}}(x,\ y)}{\sum_x \sum_y \mathrm{MWH}_{\mathrm{vein}}(x,\ y)} \cdot 100\%, \tag{15a}$$

$$\mathrm{TP}_{\mathrm{crease}} = \frac{\sum_x \sum_y \mathrm{MWH}_{\mathrm{crease}}(x,\ y) \cdot \mathrm{GT}_{\mathrm{crease}}(x,\ y)}{\sum_x \sum_y \mathrm{MWH}_{\mathrm{crease}}(x,\ y)} \cdot 100\%. \tag{15b}$$

False Positive rates can be determined from these values by means of subtraction:

$$\mathrm{FP}_{\mathrm{vein}} = 100\% - \mathrm{TP}_{\mathrm{vein}}, \tag{16a}$$

$$\mathrm{FP}_{\mathrm{crease}} = 100\% - \mathrm{TP}_{\mathrm{crease}}\,. \tag{16b}$$

A special case of FP in which we are particularly interested is when a detail of other

modality is detected. This addends of FP — vein filter detecting ridge ($\mathrm{V}\rightarrow\mathrm{C}$) and vice-versa ($\mathrm{C}\rightarrow\mathrm{V}$) are determined as follows:

$$\mathrm{FP}_{\mathrm{V}\rightarrow\mathrm{C}} = \frac{\sum_x \sum_y \mathrm{MWH}_{\mathrm{vein}}(x,\ y) \cdot (1 - \mathrm{GT}_{\mathrm{vein}}(x,\ y)) \cdot \mathrm{GT}_{\mathrm{crease}}(x,\ y)}{\sum_x \sum_y \mathrm{MWH}_{\mathrm{vein}}(x,\ y)} \cdot 100\%, \tag{17a}$$

$$\mathrm{FP}_{\mathrm{C}\rightarrow\mathrm{V}} = \frac{\sum_x \sum_y \mathrm{MWH}_{\mathrm{crease}}(x,\ y) \cdot (1 - \mathrm{GT}_{\mathrm{crease}}(x,\ y)) \cdot \mathrm{GT}_{\mathrm{vein}}(x,\ y)}{\sum_x \sum_y \mathrm{MWH}_{\mathrm{crease}}(x,\ y)} \cdot 100\%. \tag{17b}$$

6 Results and conclusions

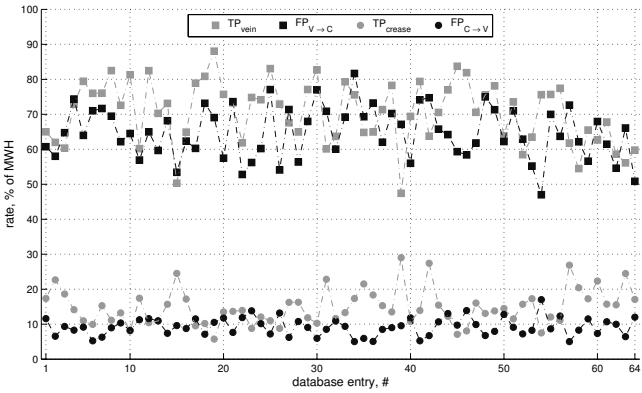

Figure 8: Evaluation results for proposed vein and crease extraction filters

The parameters described in previous section were calculated for every person in the database and are shown in figure 8. The results show the average TP rate is $70.6\ \%$ for vein detection and $64.7\ \%$ for crease detection. Corresponding average FP rates are $29.4\ \%$ and $35.3\ \%$, from which $14.8\ \%$ and $9.29\ \%$ are recognized as detection of feature of wrong modality. By analyzing these results, we can conclude that on average crease separation from veins appeared more accurate. This can be explained by the fact that creases were more clearly visible in the database images (fig. 2 shows an example), and by the fact that sometimes widest palm creases (e. g. palmar and thenar) appear visually similar to veins and, therefore, vein filter detected them.

The ground truth images contained local palm deformations due to the different palm finger placement. Therefore, pixels that were marked as ground truth could disagree with the acquired MWHs. We did not correct any local image deformations before making the experiment, however, we acknowledge that it might improve the results.

In this work we have introduced a promising biometric feature acquisition approach that offers new possibilities for multimodal biometric systems. By following the proposed procedure for image acquisition and feature extraction it is possible to simplify both — biometric device and authentication procedure. However, until a working prototype of the system will be developed, more performance tests should be performed on a broader database.

Acknowledgment

This research is partially supported by European Regional Development Fund grant No.2013/0035/2DP/2.1.1.1.0/13/APIA/VIAA/015.

References

[AEHS13] Mona A. Ahmed, M. Ebied Hala, M. Elhorbaty Elsayed, and Abdel Badeeh M. Salem. Analysis of Palm Vein Pattern Recognition Algorithms and Systems. *International Journal of Bio-Medical Informatics and e-Health*, 1(1), July 2013.

[Apt11] Aptina Imaging Corporation. *MT9V032: 1/3-Inch Wide-VGA Digital Image Sensor*, 9 2011. Rev. D.

[MCJ10] G.K.O. Michael, T. Connie, and A.T.B. Jin. Design and implementation of a contactless palm print and palm vein sensor. In *Control Automation Robotics Vision (ICARCV), 2010 11th International Conference on*, pages 1268–1273, Dec 2010.

[PFG13] M. Pudzs, R. Fuksis, and M. Greitans. Palmprint image processing with Non-Halo Complex Matched Filters for forensic data analysis. In *Biometrics and Forensics (IWBF), 2013 International Workshop on*, pages 1–4, April 2013.

[PFR+13] M. Pudzs, R. Fuksis, R. Ruskuls, T. Eglitis, A. Kadikis, and M. Greitans. FPGA based palmprint and palm vein biometric system. In *Biometrics Special Interest Group (BIOSIG), 2013 International Conference of the*, pages 1–4, Sept 2013.

[PGF11] M. Pudzs, M. Greitans, and R. Fuksis. Complex 2D matched filtering without Halo artifacts. In *Systems, Signals and Image Processing (IWSSIP), 2011 18th International Conference on*, pages 1–4, June 2011.

[SB99] J. Swarbrick and C. J. Boylan. *Encyclopedia of Pharmaceutical Technology*, volume 19. Informa Health Care Blood Substitutes: Hemoglobin based Oxygen Carriers to Tablet Evaluation Using Near Infrared Spectroscopy, page 500, 1999.

[Tru12] Truesense Imaging Inc. *Reference Document: Image Sensor Color Correction*, 8 2012.

[WESS05] M. Watanabe, T. Endoh, M. Shiohara, and S Sasaki. Palm vein authentication technology and its applications. In *Proceedings of The Biometric Consortium Conference*, pages 1–2, Sept 2005.